

Fault-controlled hydration of the upper mantle during continental rifting

Bayracki, Gaye; Minshull, Tim; Sawyer, Dale; Reston, Timothy; Klaeschen, Dirk; Papenberg, Cord; Ranero, Cesar; Bull, Jonathan; Davy, Richard; Shillington, Donna; Perez Gussinye, Marta; Morgan, Julia

DOI:
[10.1038/ngeo2671](https://doi.org/10.1038/ngeo2671)

License:
None: All rights reserved

Document Version
Peer reviewed version

Citation for published version (Harvard):
Bayracki, G, Minshull, T, Sawyer, D, Reston, T, Klaeschen, D, Papenberg, C, Ranero, C, Bull, J, Davy, R, Shillington, D, Perez Gussinye, M & Morgan, J 2016, 'Fault-controlled hydration of the upper mantle during continental rifting', *Nature Geoscience*, vol. 9, pp. 384-388. <https://doi.org/10.1038/ngeo2671>

[Link to publication on Research at Birmingham portal](#)

Publisher Rights Statement:
Checked for eligibility: 05/04/2016. Published in Nature Geoscience.

General rights

Unless a licence is specified above, all rights (including copyright and moral rights) in this document are retained by the authors and/or the copyright holders. The express permission of the copyright holder must be obtained for any use of this material other than for purposes permitted by law.

- Users may freely distribute the URL that is used to identify this publication.
- Users may download and/or print one copy of the publication from the University of Birmingham research portal for the purpose of private study or non-commercial research.
- User may use extracts from the document in line with the concept of 'fair dealing' under the Copyright, Designs and Patents Act 1988 (?)
- Users may not further distribute the material nor use it for the purposes of commercial gain.

Where a licence is displayed above, please note the terms and conditions of the licence govern your use of this document.

When citing, please reference the published version.

Take down policy

While the University of Birmingham exercises care and attention in making items available there are rare occasions when an item has been uploaded in error or has been deemed to be commercially or otherwise sensitive.

If you believe that this is the case for this document, please contact UBIRA@lists.bham.ac.uk providing details and we will remove access to the work immediately and investigate.

1 **Fault-controlled hydration of the upper mantle during continental rifting**

2
3 G. Bayrakci¹, T. A. Minshull^{1*}, D. S. Sawyer², T. J. Reston³, D. Klaeschen⁴, C.
4 Papenberg⁴, C. Ranero⁵, J. M. Bull¹, R. G. Davy¹, D. J. Shillington⁶, M. Perez-
5 Gussinye⁷, J. K. Morgan²

6
7 1- University of Southampton, Ocean and Earth Science, National Oceanography Centre
8 Southampton, Southampton, United Kingdom

9 2- Rice University, Department of Earth Science, Houston, United States

10 3- University of Birmingham, School of Geography, Earth and Environmental Sciences,
11 Birmingham, United Kingdom

12 4- GEOMAR, Helmholtz Centre for Ocean Research Kiel, Marine Geodynamics, Kiel,
13 Germany

14 5- ICREA at CSIC, Barcelona Centre for Subsurface Imaging, Instituto de Ciencias del
15 Mar, Barcelona, Spain

16 6- Lamont-Doherty Earth Observatory of Columbia University, Marine Geophysics,
17 Palisades, United States

18 7- Royal Holloway University of London, Department of Earth Sciences, London,
19 United Kingdom

20
21
22 **Water and carbon are transferred from the ocean to the mantle in a process that**
23 **alters mantle peridotite to create serpentinite and supports diverse**
24 **ecosystems¹. Serpentinised mantle rocks are found beneath the seafloor at slow- to**
25 **ultraslow-spreading mid-ocean ridges¹ and are thought to be present at about half**
26 **the world's rifted margins^{2,3}. Serpentinite is also inferred to exist in the downgoing**

27 **plate at subduction zones⁴, where it may trigger arc magmatism or hydrate the**
28 **deep Earth. Water is thought to reach the mantle via active faults^{3,4}. Here we show**
29 **that serpentinitisation at the rifted continental margin offshore from western Spain**
30 **was probably initiated when the whole crust cooled to become brittle and**
31 **deformation was focused along large normal faults. We use seismic tomography to**
32 **image the three-dimensional distribution of serpentinitisation in the mantle and find**
33 **that the local volume of serpentinite beneath thinned, brittle crust is related to the**
34 **amount of displacement along each fault. This implies that seawater reaches the**
35 **mantle only when the faults are active. We estimate the fluid flux along the faults**
36 **and find it is comparable to that inferred for mid-ocean ridge hydrothermal**
37 **systems. We conclude that brittle processes in the crust may ultimately control the**
38 **global flux of seawater into the Earth.**

39
40 The formation of serpentinite requires a supply of fluids to the mantle, but the bulk
41 continental crust typically has low permeabilities (10^{-14} to 10^{-18} m²)⁽⁵⁾. Active faults
42 have been shown to transmit fluids during earthquakes and fault damage zones form
43 potential fluid pathways⁶, but low-permeability fault gouge can be a barrier to fluid
44 flow⁷. In short, the complex distribution of low and high permeability features within
45 fault zones leads to extreme permeability heterogeneity and anisotropy⁷, so that the
46 importance of faults as fluid pathways over geological timescales is unclear.

47
48 During rifting at magma-poor continental margins, crustal thinning leads to a reduction
49 in overburden pressure at depth, which together with cooling moves the originally
50 viscous lower crust into the brittle field³. Numerical models that track the thermal and
51 rheological evolution of rifted margins have suggested that, for a wide range of strain
52 rates and starting rheologies, the entire crust should become brittle at thicknesses of

53 between 14 and 4 km (Fig. 1a). Sufficient coincident deep seismic reflection and
54 refraction profiles across magma-poor rifted margins now exist to enable a rigorous
55 comparison between the observed maximum crustal thickness above or juxtaposed
56 against serpentinised mantle, and the thickness at which complete crustal embrittlement
57 is expected to occur⁸ (Fig. 1 and Supplementary Fig. S1; Methods). Our compilation
58 shows that serpentinite is found only where the crust is thin enough to have become
59 entirely brittle during rifting and for many margins, such as Porcupine Basin⁹ and
60 Southeast Flemish Cap¹⁰, conjugate to Galicia margin the predictions exactly match the
61 observations (Fig. 1a-c and Supplementary Fig. S1). At some margins (e.g., Nova
62 Scotia¹¹; Fig. 1e and Supplementary Fig. S1) serpentinite only occurs beneath crust
63 both thinner and some distance oceanward than predicted. However, in each case thick
64 synrift sediments and/or salt, both known to reduce permeability¹², are present. It is
65 clear that a brittle crust is not the only criterion for the serpentinisation; suitable fluid
66 pathways must also exist. Perhaps most intriguingly, at other margins, the misfit is small,
67 with serpentinite only occurring under crust that is thinner than predicted but only about
68 a fault block spacing (5-10 km) further oceanward than predicted (Figs. 1a and d,
69 Supplementary Fig. S1). This observation suggests that the serpentinisation process may
70 be controlled by faults cutting down from the seafloor to the mantle. Thus at all
71 serpentinite margins, where block bounding normal faults are well imaged, there is a
72 strong link between the presence and the spacing of the brittle faulting in the thin crust
73 and the serpentinisation of the underlying mantle.

74
75 The Deep Galicia segment of the magma-poor west Iberia rifted margin (Figs 1 and 2d)
76 is one such margin. Here, rifting led to the formation of hyperextended continental crust
77 with serpentinisation, detachment faulting and subsequent mantle exhumation¹³.
78 Serpentinite has a lower density and coefficient of friction than fresh mantle peridotite

79 and causes weakening of the mantle¹⁴. The most recent normal faults soled out into the
80 weaker serpentinite layer, forming a detachment-like surface at the boundary between
81 the fault-bounded tilted crustal blocks and serpentinised mantle, a boundary described
82 from seismic reflection profiles as the “S reflector”¹³.

83
84 We compare the 3D compressional (P-) wave velocity structure of the Deep Galicia
85 Margin obtained from first-arrival travel-time tomography (Methods) with tectonic
86 structure from representative pre-stack depth migrated multi-channel seismic reflection
87 profiles, migrated using independent velocity models (Fig. 2). We obtained velocities
88 similar to those previously obtained from a two-dimensional transect through the same
89 area¹⁵, but our denser sampling and 3D survey geometry (Supplementary Figs. S2 and
90 S3) yield much improved resolution. The smooth velocity model closely matches the 5-
91 10 km wide tilted basement blocks imaged on the seismic profiles. From the interpreted
92 top of the crystalline basement down to the S reflector, velocities vary between 5.5 and
93 6.5 km/s; the 6.5 km/s iso-velocity contour follows closely the S reflector where it
94 underlies the tilted basement blocks (root-mean-square difference 0.4 km), illustrating
95 the resolution of the model, confirmed using standard resolution tests (Supplementary
96 Information, Supplementary Figs. S4 - S7) for velocities both above and below S.
97 Velocities beneath the S reflector increase to 7.5 km/s over a mean depth interval of 1.2
98 km. If these velocity variations are attributed solely to variations in the degree of
99 serpentinisation, they would correspond to a decrease from ~45% serpentinisation (6%
100 by weight of water) immediately below the S reflector to ~15% at depths of ~1.2 km
101 below the S reflector. The inversion yields a smooth, isotropic model. Anisotropy is
102 likely to be present in the uppermost mantle but limited to a few per cent when
103 velocities are reduced by serpentinisation to 6.5-7.5 km/s¹⁶.

104

105 Intriguingly, at the intersections between the block-bounding normal faults and the S
106 reflector, this velocity increase occurs over a larger depth interval (~2 km), suggesting a
107 locally thicker zone of highly serpentinised mantle (Figs. 2 and 3a). This observation
108 implies that faults in the hanging-wall of the S reflector have had a role in the transport
109 of seawater to the mantle. Alternatively, velocities could be reduced by the presence
110 beneath S of lower crustal material or of frozen melt. However, lower crustal material is
111 unlikely because none is imaged on coincident seismic reflection profiles, and mafic
112 intrusions are also unlikely as no magmatism is known at this margin, and we would not
113 expect its location to be controlled by faulting processes above S.

114
115 The volume of seawater supplied to the mantle has been estimated from the volume of
116 the serpentinised region and the degree of serpentinisation (Methods). Each block-
117 bounding fault is associated with a maximum in water uptake, implying not only that the
118 water uptake was controlled by the deformation associated with those faults but also that
119 the serpentinised mantle has subsequently moved with the overlying fault blocks,
120 requiring the S detachment progressively to have become inactive, as expected for
121 brittle sequential faulting¹⁷ such as in rolling hinge model¹⁸. Hydrothermal systems
122 commonly involve focused upflow along faults and diffuse downflow away from
123 faults¹⁹. Our data only tell us the water volume required for the observed degree of
124 serpentinisation, from which we infer the total net downflow during serpentinisation
125 (Methods). The inferred net downflow (minimum time-integrated flux) for individual
126 faults varies between 1.2×10^4 and 5.9×10^4 m³ per square metre of fault cross-sectional
127 area. There are very few published estimates for comparison, but our estimated time
128 integrated fluxes are comparable to values of $\sim 10^5$ m³/m² inferred for mid-ocean ridge
129 faults in the Oman Ophiolite²⁰.

130

131 Along the southernmost profile the fault that intersects the S reflector beneath the basin
132 oceanward of the last continental fault block (Supplementary Fig. S8c, F6, profile ISE1),
133 is not used for the estimation of time integrated fluxes. At that location the observed
134 high degree of serpentinisation may be due to the direct connection at breakup time
135 between the ocean and the exhumed foot-wall mantle. This environment may have been
136 similar to off-axis, low-temperature, ultra-mafic hosted foot-wall hydrothermal systems
137 observed at mid-ocean ridges²¹.

138

139 The strong correlation between the water volumes and the fault displacements
140 (correlation coefficient: 0.91, probability of no correlation: 0.006; Fig. 3c and
141 Supplementary Figs. S9 - S10; Methods) suggests that a physical process links these
142 parameters, perhaps associated with increased connectivity of fluid pathways when
143 faults move²². If we assume that the faults above the S reflector moved sequentially to
144 accommodate a constant extension rate¹⁷, the duration of their activity, and therefore the
145 corresponding flow rates, may be inferred from their displacement (Methods). Inferred
146 flow rates vary between 6.2×10^{-8} and $3.8 \times 10^{-7} \text{ m}^3 \text{ s}^{-1}$ per metre along the rift. These rates
147 are around one order of magnitude less than those associated with high-temperature
148 fluid fluxes at the TAG hydrothermal field, where a flux of $\sim 100 \text{ kg/s}$ ⁽²³⁾ is inferred to
149 be sourced from 35-61 km of rift²⁴, corresponding to a flow rate of $2\text{-}3 \times 10^{-6} \text{ m}^3 \text{ s}^{-1}$ per
150 metre.

151

152 Water circulation in the crust may be driven by episodic changes in tectonic stress and
153 in fault zone permeability⁶. A combination of coupled fluid pressure and mean stress,
154 suction pumping action and fault-valve action leads to the cyclic accumulation of water,
155 followed by fault reactivation and release of fluids²⁵. Rather than using the fault
156 damage zone, the downflow may occur through antithetic faults created at the tips of

157 normal faults when they penetrate into regions of reduced yield stress⁶, with any upflow
158 through the fault damage zone. At the Deep Galicia Margin such antithetic faults might
159 have started to form where the normal faults sole out onto the S reflector detachment
160 surface. As the opening of such antithetic faults is driven by the slip cycle on the main
161 block-bounding fault, fluid flow will also be proportional to the slip on that fault,
162 explaining the fit in Figure 3c. This latter mechanism may explain why serpentinisation
163 appears to be focused beneath the hanging-walls of the normal faults detaching onto S
164 (Fig. 2).

165
166 We do not infer 100% serpentinisation anywhere below the S reflector. The production
167 of new serpentinite depends on the temperature of the medium and the access of the
168 water to the unreacted peridotite, which is controlled by the water supply and the
169 porosity and the permeability of the medium^{26,27}. Serpentinite has a lower permeability
170 (10^{-23} - 10^{-22} m²) than crustal rocks and faults and serpentinisation is a volume-increasing
171 process (up to 40% of volume expansion^{3,27}) that reduces the initial rock porosity to
172 near zero. However, due to the volume expansion, cracking occurs and locally increases
173 the permeability. Within the serpentinite the water flow uses these cracks and is driven
174 by the pressure gradient created by the serpentinisation²⁷. The incomplete
175 serpentinisation may suggest an insufficient water supply, in which case all of the
176 available water may have been consumed.

177
178 Alternatively, high temperatures and/or the limited access of the water to fresh mantle
179 peridotite may have resulted in a low serpentinisation rate. In that case, the water may
180 have been recycled by upflow along the faults. At the onset of serpentinisation during
181 continental breakup, the crust is less than 14 km thick (Fig. 1a), and the mantle is at
182 around 400-500 °C, i.e. the upper limit of the serpentinite stability²⁶. The geothermal

183 gradient is high and remains high due to heat released during serpentinisation, providing
184 suitable conditions for focused upflow along the fault damage zones. If such
185 hydrothermal circulation is initiated, it will continue until the pore-filling reactions
186 between the hydrothermal fluids and the cold crustal rocks and ambient fluids lower the
187 damage zone permeability again²².

188

189 Here we quantified the fluid fluxes in a rifted margin setting, but our approach could
190 also be at mid-ocean ridges and subduction zones given seismic data of sufficient
191 resolution. Our results show that when the entire crust becomes brittle during extension,
192 bulk serpentinisation in the upper 2 km of the mantle is enhanced close to crustal faults,
193 and thus that hydration of the upper mantle is fault-controlled. Therefore brittle
194 processes in the crust ultimately may control the global flux of seawater into the solid
195 Earth.

196

197 **References**

198

199 1. Fruh-Green, G.L., et al., *Serpentinization of oceanic peridotites: Implications for*
200 *geochemical cycles and biological activity*. *Subseafloor Biosphere at Mid-Ocean*
201 *Ranges*, 2004. **144**: p. 119-136.

202 2. Whitmarsh, R.B., et al., *Tectonic implications of exposure of lower continental crust*
203 *beneath the Iberia Abyssal Plain, Northeast Atlantic Ocean: Geophysical evidence*.
204 *Tectonics*, 2000. **19**(5): p. 919-942.

205 3. Perez-Gussinye, M. and T.J. Reston, *Rheological evolution during extension at*
206 *nonvolcanic rifted margins: Onset of serpentinization and development of detachments*
207 *leading to continental breakup*. *Journal of Geophysical Research-Solid Earth*, 2001.
208 **106**(B3): p. 3961-3975.

209 4. Ranero, C.R., et al., *Bending-related faulting and mantle serpentinization at the Middle*
210 *America trench*. *Nature*, 2003. **425**(6956): p. 367-373.

211 5. Manning, C.E. and S.E. Ingebritsen, *Permeability of the continental crust: Implications*
212 *of geothermal data and metamorphic systems*. *Reviews of Geophysics*, 1999. **37**(1): p.
213 127-150.

214 6. Sibson, R.H., *Fluid involvement in normal faulting*. *Journal of Geodynamics*, 2000.
215 **29**(3-5): p. 469-499.

216 7. Faulkner, D.R., et al., *A review of recent developments concerning the structure,*
217 *mechanics and fluid flow properties of fault zones*. *Journal of Structural Geology*, 2010.
218 **32**(11): p. 1557-1575.

219 8. Reston, T.J., *The structure, evolution and symmetry of the magma-poor rifted margins*
220 *of the North and Central Atlantic: A synthesis*. *Tectonophysics*, 2009. **468**(1-4): p. 6-27.

221 9. O'reilly, B.M., et al., *Crustal thinning, mantle exhumation and serpentinization in the*
222 *Porcupine Basin, offshore Ireland: evidence from wide-angle seismic data*. *Journal of*

- 223 the Geological Society, 2006. **163**: p. 775-787.
- 224 10. Funck, T., et al., *Crustal structure of the ocean-continent transition at Flemish Cap:*
225 *Seismic refraction results*. Journal of Geophysical Research-Solid Earth, 2003.
226 **108**(B11).
- 227 11. Zelt, C.A., et al., *Assessment of crustal velocity models using seismic refraction and*
228 *reflection tomography (vol 153, pg 609, 2003)*. Geophysical Journal International, 2003.
229 **154**(1): p. 230-230.
- 230 12. Wu, Y., et al., *Crustal structure of the central Nova Scotia margin off Eastern Canada.*
231 Geophysical Journal International, 2006. **166**(2): p. 878-906.
- 232 13. Rupke, L.H., et al., *Interrelation between rifting, faulting, sedimentation, and mantle*
233 *serpentinization during continental margin formation-including examples from the*
234 *Norwegian*. Geochemistry Geophysics Geosystems, 2013. **14**(10): p. 4351-4369.
- 235 14. Reston, T.J., et al., *Movement along a low-angle normal fault: The S reflector west of*
236 *Spain*. Geochemistry Geophysics Geosystems, 2007. **8**.
- 237 15. Escartin, J., G. Hirth, and B. Evans, *Effects of serpentinization on the lithospheric*
238 *strength and the style of normal faulting at slow-spreading ridges*. Earth and Planetary
239 Science Letters, 1997. **151**(3-4): p. 181-189.
- 240 16. Ranero, C.R. and M. Perez-Gussinye, *Sequential faulting explains the asymmetry and*
241 *extension discrepancy of conjugate margins*. Nature, 2010. **468**(7321): p. 294-U180.
- 242 17. Borgmeyer, A.L., *Three-dimensional geometries of rifting on a hyperextended margin -*
243 *Interpretation of seismic reflection profiles from the Deep Galicia Basin, Iberia*. 2010,
244 Rice University.
- 245 18. Christensen, N.I., *Serpentinites, peridotites, and seismology*. International Geology
246 Review, 2004. **46**(9): p. 795-816.
- 247 19. Buck, W.R., *Flexural rotation of normal faults*. Tectonics, 1988. **7**(5): p. 959-973.
- 248 20. Kelley, D.S., J.A. Baross, and J.R. Delaney, *Volcanoes, fluids, and life at mid-ocean*

- 249 *ridge spreading centers*. Annual Review of Earth and Planetary Sciences, (2002) **30(1)**,
250 **385-491**.
- 251 21. Coogan, L.A., et al., *Chemical and thermal constraints on focussed fluid flow in the*
252 *lower oceanic crust*. American Journal of Science, 2006. **306(6)**: p. 389-427.
- 253 22. Fruh-Green, G.L., et al., *30,000 years of hydrothermal activity at the Lost City vent field*.
254 Science, 2003. **301(5632)**: p. 495-498.
- 255 23. Reynolds, S.J. and G.S. Lister, *Structural Aspects of Fluid-Rock Interactions in*
256 *Detachment Zones*. Geology, 1987. **15(4)**: p. 362-366.
- 257 24. Hannington, M.D., et al, *Comparison of the TAG mound and stockwork complex with*
258 *Cyprus-type massive sulphide deposit*. . Proceedings of the Ocean Drilling Program,
259 Scientific Results, 1998. **158**: p. 389-415.
- 260 25. Baker, E.T., *Hydrothermal cooling of midocean ridge axes: Do measured and modeled*
261 *heat fluxes agree?*, *Earth and Planetary Science Letters*. 2007 **263**,(1-2): p. 40-150.
- 262 26. Sibson, R.H., *Generation of Pseudotachylyte by Ancient Seismic Faulting*. Geophysical
263 Journal of the Royal Astronomical Society, 1975. **43(3)**: p. 775-&.
- 264 27. Emmanuel, S. and B. Berkowitz, *Suppression and stimulation of seafloor hydrothermal*
265 *convection by exothermic mineral hydration*. Earth and Planetary Science Letters, 2006.
266 **243(3-4)**: p. 657-668.
- 267 28. Macdonald, A.H. and W.S. Fyfe, *Rate of Serpentinization in Seafloor Environments*.
268 Tectonophysics, 1985. **116(1-2)**: p. 123-135.

269

270

271 **Acknowledgements**

272 We thank all who sailed with us on *R/V Marcus Langseth* and *F/S Poseidon* for their
273 hard work at sea, Marianne Karplus for assistance with detailed survey design and Anne
274 Krabbenhoft for assistance with data processing. This research was supported by the
275 US National Science Foundation, the UK Natural Environment Research Council
276 (NE/E016502/1) and GEOMAR Helmholtz Centre for Ocean Research. Ocean bottom
277 instruments were provided by the UK Ocean Bottom Instrumentation Facility and by
278 GEOMAR. T.A.M. was supported by a Wolfson Research Merit award.

279

280 **Author Contributions**

281 D.S.S., T.J.R., T.A.M., D.K., D.J.S., C.R., J.B. and J.K.M. designed the seismic
282 experiment. D.S.S. led the survey on *R/V Marcus Langseth* and D.K. and C.P. led the
283 deployment and recovery of seafloor instruments aboard *F/S Poseidon*. G.B. conducted
284 the seismic data analysis, with some assistance from R.G.D. T. J. R. compiled the
285 North Atlantic seismic profiles and M.P.G. carried out the numerical modelling. G.B.
286 and T.A.M. wrote the first draft of the paper and all authors contributed to subsequent
287 revisions.

288

289 **Additional Information**

290 Supplementary information is available in the online version of the paper. Reprints and
291 permissions information is available online at www.nature.com/reprints.
292 Correspondence and requests for materials should be addressed to T.A.M

293

294 **Competing financial interests**

295 The authors have no competing financial interests.

296

297 **Figure Legends**

298 **Figure 1: a)** Comparison between the crustal thickness at which complete crustal
299 embrittlement is predicted to occur³ (grey region covering three different modelled
300 rheologies) and the maximum crustal thickness observed above or juxtaposed against
301 serpentinised mantle at various North Atlantic magma-poor margins⁸. NS: Nova Scotia,
302 PB: Porcupine Basin, FC: Flemish Cap, IAP: Iberian Abyssal Plain, ARM: Armorican
303 Margin, NB: Newfoundland Basin, TAP: Tagus Abyssal Plain. The prefixes W, E, N, S
304 are West, East, North and South respectively. Cross sections of **b)** Porcupine Basin⁹, **c)**
305 Southeast Flemish Cap¹⁰, **d)** Galicia¹⁵ and **e)** Nova Scotia¹¹ margins.

306
307 **Figure 2:** Compressional (P-) wave velocities superimposed on coincident seismic
308 reflection profiles illustrate the concentration of serpentinisation beneath the hanging-
309 wall of normal faults (expansion of 6.5 – 7.5 km/s iso-velocity interval). Yellow circles
310 are seabed instrument locations. Iso-velocity contours are marked by thin black lines.
311 Dashed lines mark the seabed (pale blue), interpreted base of post-rift sediments (green),
312 top of the pre-rift sediments (blue), top of the crystalline basement (red), S reflector
313 (black). Thick black lines indicate faults. **a)** ISE4 profile¹³; **b)** IAM 11 profile¹⁷; **c)** ISE1
314 profile²⁸; **d)** location of the Galicia 3D survey with colour-coded bathymetry. **e)**
315 Schematic illustrating serpentinization associated with a single normal fault "F".

316
317 **Figure 3:** Water volume and amount of serpentinisation associated with faults on the
318 seismic reflection profile shown in Fig. 2b, assuming a two-dimensional structure. **a)**
319 Degree of serpentinisation (white contours) and water content (black contours). Black
320 and green boxes show the vertical and horizontal integration domains, respectively.
321 Bold black lines are the faults and dashed black line is the S reflector. **b)** Vertically
322 integrated water content (black) and horizontal extent associated with faults (green). **c)**

323 Correlation between water volume within hydrated mantle, representing integrated net
324 fluid flux through the fault, and fault displacement at the top of crystalline basement.
325 Data derived from seismic profiles (Fig. 2a – c) are shown by the magenta, green and
326 blue colors respectively. Faults F4 – F6 are shown by the triangle, square and circle
327 symbols respectively.

328

329

330 **Methods**

331 We calculated the stretching factor at which the entire crust becomes brittle using
332 hundreds of runs of a one-dimensional numerical model, in which a 125-km lithosphere
333 with a 32 km crust undergoes extension by a uniform pure strain rate³. The initial basal
334 and Moho temperatures were 1300° of 550° C, respectively³. We used a wet quartz
335 rheology for the upper crust, anorthosite, dry quartz and aggregate rheologies for the
336 lower crust, and a dry olivine rheology for the mantle³. For various Atlantic rifted
337 margins, we used published profiles showing the depth to the top of crystalline crust
338 from seismic reflection data and the depth to the Moho and distribution of mantle
339 serpentinisation from wide-angle seismic data (Supplementary Fig. S1). From these
340 profiles, we determined the maximum crustal thickness either beneath which detectable
341 serpentinisation occurs (e.g. Galicia), or where crust and serpentinite are juxtaposed (e.g.
342 S Iberia Abyssal Plain).

343
344 Seismic data on the Deep Galicia Margin were collected between June and September
345 2013. The primary aim of the survey was to acquire a three-dimensional seismic
346 reflection volume. Airgun shots were fired from *R/V Marcus Langseth* along fifty
347 parallel profiles with 400 m spacing between them (Supplementary Fig. S2), alternating
348 between two 3000 cu. in. airgun arrays to give a shot interval of 37.5 m (~16 s). A grid
349 of 72 ocean bottom instruments, comprising 44 four-component ocean bottom
350 seismometers (OBSs) and 28 ocean bottom hydrophones (OBHs) was deployed on the
351 seabed for three months to record these shots, with sample rates of 250 Hz and 200 Hz,
352 respectively. OBS/H data were corrected for internal clock drifts and instruments were
353 relocated using a 2D iterative inversion (Supplementary Information). In our analysis
354 we used first arrival travel-times from 48 OBS/H spread across the survey area
355 (Supplementary Fig. S2). The pick uncertainty was estimated visually as a function of

356 signal noise ratio and varied from 50 to 230 ms.

357

358 The P-wave velocity image was constructed using a non-linear iterative tomographic
359 technique (FAST²⁹). A total of 155,924 first arrival times was used, corresponding
360 mostly to crustal refractions, since there are few first arrivals from shallower parts of the
361 structure (Supplementary Fig. S3). We used a forward grid of 0.5 km node interval and
362 an inverse grid of 1 km cell size. The starting models used in this study and the
363 resolution and uncertainty of the inversion results are discussed in the Supplementary
364 Information (Supplementary Figs. S4 – S7).

365

366 P-wave velocities were converted to percentage of serpentinization below the depth of
367 the S reflector and the water content by weight was estimated using an empirical
368 relationship³⁰ (Fig. 3 and Supplementary Fig. S8). The water content may be
369 overestimated because of model smoothing across a velocity discontinuity. The weight
370 of serpentinite was calculated using the estimated density of the serpentinite at each grid
371 node and the water weight percentages were used to calculate the water volume. The
372 water volume associated with a given block-bounding normal fault was estimated by
373 integrating the water volume over a vertical interval of 2.5 km beneath the S reflector
374 and a horizontal interval of 7 km (Fig. 3 and Supplementary Fig. S8). The bottom of the
375 depth interval was chosen to be close to the limit of ray coverage (Supplementary Fig.
376 S5). The horizontal integration interval approximates the width of the region of reduced
377 velocities around an isolated fault (Figs 2b and 3a, F5, profile IAM 11). The values
378 resulting from the vertical and horizontal integration (Fig. 3c) represent the water
379 volume per unit length along the margin that is associated with a given fault. Some of
380 this fluid will have been fed by the S detachment itself, perhaps represented by the
381 intercept on the vertical axis of the regression line shown in Fig. 3c. The minimum time-

382 integrated fluxes are estimated by dividing the water content associated with the faults
383 by the thickness of the faults. A thickness of 50 m was inferred for the S reflector by the
384 full waveform inversion along profile ISE1³¹, and for this approximate calculation we
385 assume that the block-bounding faults have comparable thickness.

386

387 Fault displacements at the top of crystalline basement were estimated from foot-wall
388 and hanging-wall cut-off³² measured for each fault block, on pre-stack depth migrated
389 seismic profiles (Fig. 2a-c and Supplementary Fig. S9). Due to the topography of the
390 crystalline basement, a minimum and a maximum displacement were calculated for
391 each fault and the mean displacement was used in the discussion. Water content
392 estimation errors were calculated using the standard deviations of the P-wave velocity at
393 the nodes (Fig. 3c and Supplementary Fig. S7). We estimated the duration of activity of
394 the faults by dividing the heaves by the half extension rate of 0.8 ± 0.36 cm/yr³³. We then
395 estimated the flow rates by dividing the water volume related with one fault by the
396 duration of activity of that fault.

397

398 **Code Availability:** The tomographic FAST²⁹ code used for this study is available at
399 <http://terra.rice.edu/department/faculty/zelt/fast.html>

400

401

- 402 29. Zelt, C.A. and P.J. Barton, *Three-dimensional seismic refraction tomography: A*
403 *comparison of two methods applied to data from the Faeroe Basin*. Journal of
404 Geophysical Research-Solid Earth, 1998. **103**(B4): p. 7187-7210.
- 405 30. Carlson, R.L. and D.J. Miller, *Mantle wedge water contents estimated from seismic*
406 *velocities in partially serpentinitized peridotites*. Geophysical Research Letters, 2003.
407 **30**(5).
- 408 31. Leythaeuser, T., T.J. Reston, and T.A. Minshull, *Waveform inversion of the S reflector*
409 *west of Spain: Fine structure of a detachment fault*. Geophysical Research Letters, 2005.
410 **32**(22).
- 411 32. Mansfield, C. and J. Cartwright, *Fault growth by linkage: observations and implications*
412 *from analogue models*. Journal of Structural Geology, 2001. **23**(5): p. 745-763.
- 413 33. Sutra, E., et al., *Quantification and restoration of extensional deformation along the*
414 *Western Iberia and Newfoundland rifted margins*. Geochemistry Geophysics
415 Geosystems, 2013. **14**(8): p. 2575-2597.
- 416

Figures

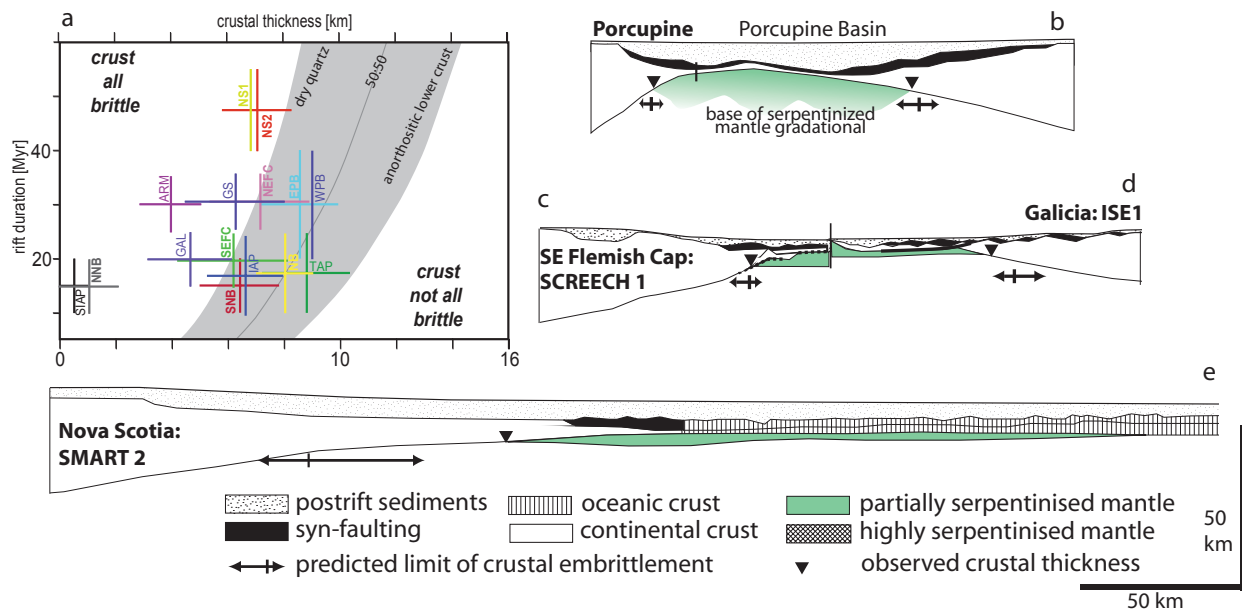


Figure 1: Comparison between the crustal thickness at which complete crustal embrittlement is predicted to occur³ and the maximum crustal thickness observed above or juxtaposed against serpentinitised mantle at various a) Modelling results showing the crustal thickness at which the entire crust becomes brittle (grey region covering three different modelled rheologies). North Atlantic magma-poor margins⁸. NS: Nova Scotia, PB: Porcupine Basin, FC: Flemish Cap, IAP: Iberian Abyssal Plain, GS: Goban Spur, ARM: Armorican Margin, GAL: Galicia, NB: Newfoundland Basin, TAP: Tagus Abyssal Plain. The prefixes W, E, N, S are West, East, North and South respectively. Cross sections of b) Porcupine Basin⁹, c) Southeast Flemish Cap¹⁰, profile SCREECH-1, d) Galicia¹¹, profile ISE-1, and e) Nova Scotia¹², profile SMART-2.

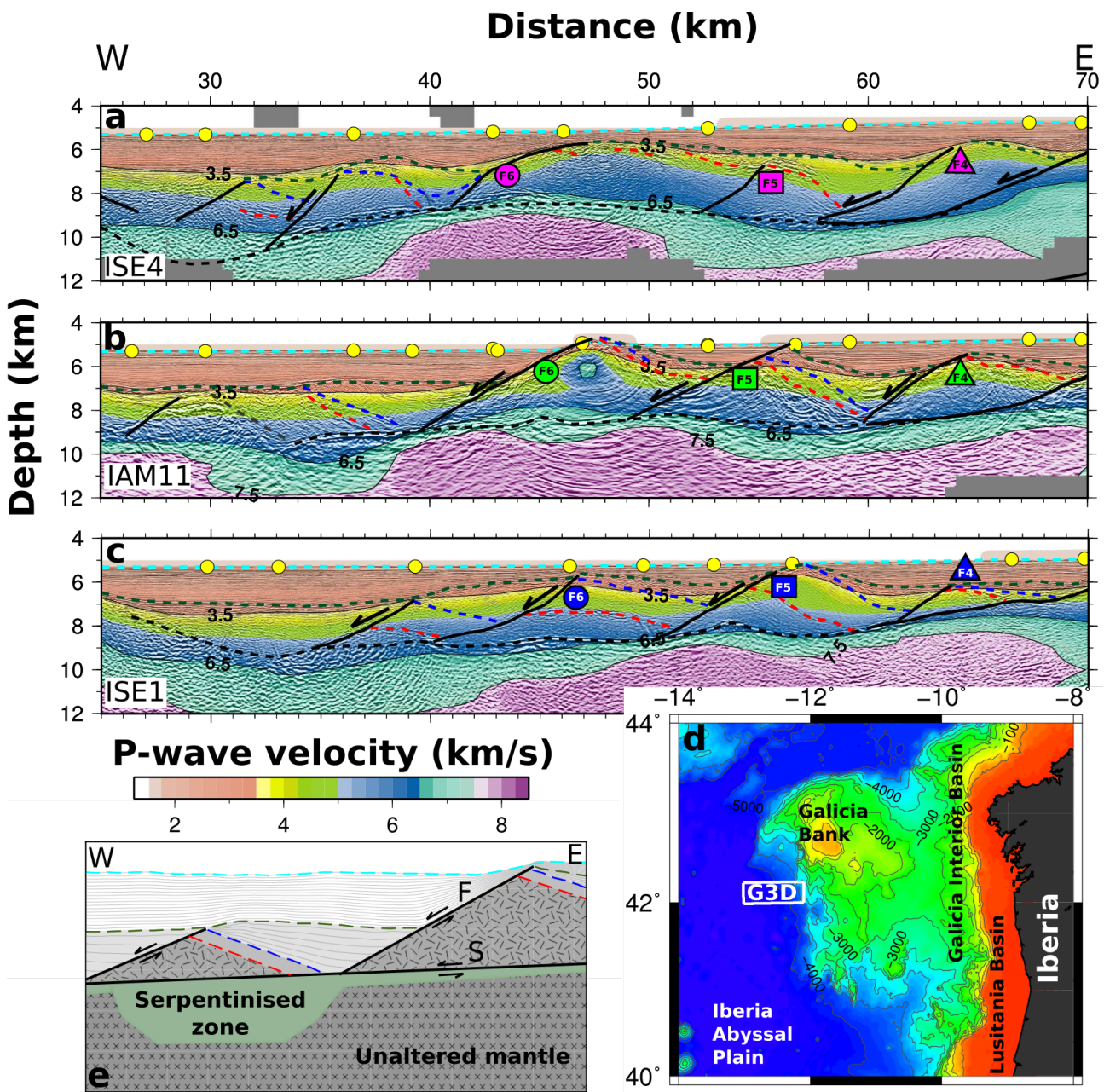


Figure 2: Compressional (P-) wave velocities superimposed on coincident seismic reflection profiles illustrate the concentration of serpentinisation beneath the hanging-wall of normal faults (expansion of 6.5 – 7.5 km/s iso-velocity interval). Yellow circles are seabed instrument locations. Iso-velocity contours are marked by thin black lines. Dashed lines mark the seabed (pale blue), interpreted base of post-rift sediments (green), top of the pre-rift sediments (blue), top of the crystalline basement (red), S reflector (black). Thick black lines indicate faults. **a)** ISE4 profile¹⁴; **b)** IAM 11 profile¹⁶; **c)** ISE1 profile¹⁷; **d)** location of the Galicia 3D survey with colour-coded bathymetry. **e)** Schematic illustrating serpentinization associated with a single normal fault "F".

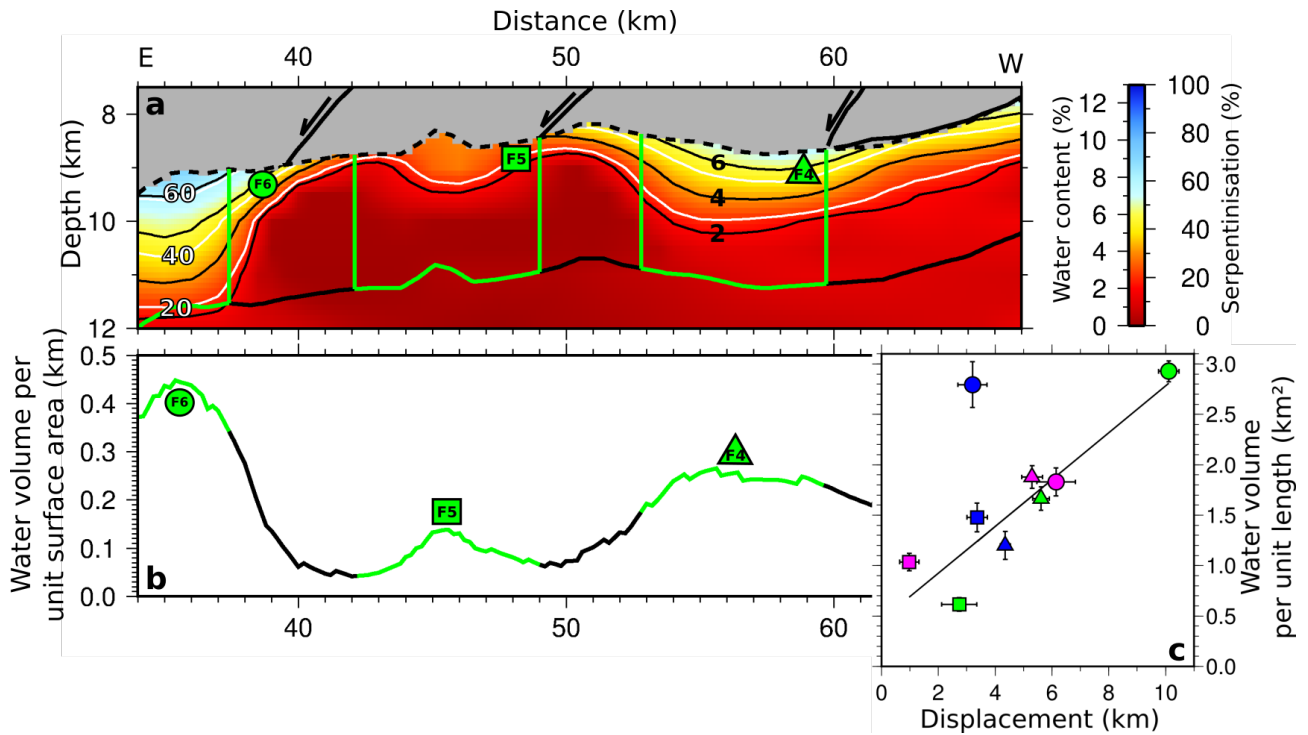


Figure 3: Water volume and amount of serpentinisation associated with faults on the seismic reflection profile shown in Fig. 2b, assuming a two-dimensional structure. **a)** Degree of serpentinisation (white contours) and water content (black contours). Black and green boxes show the vertical and horizontal integration domains, respectively. Bold black lines are the faults and dashed black line is the S reflector. **b)** Vertically integrated water content (black) and horizontal extent associated with faults (green). **c)** Correlation between water volume within hydrated mantle, representing integrated net fluid flux through the fault, and fault displacement at the top of crystalline basement. Data derived from seismic profiles (Fig. 2a – c) are shown by the magenta, green and blue colors respectively. Faults F4 – F6 are shown by the triangle, square and circle symbols respectively.